CdTe Semiconductor Nanowires and NiFe Ferro-magnetic Metal Nanowires Electrodeposited into the Cylindrical Nano-Pores on the Surface of Metallic Aluminum

Takeshi Ohgai*, Laurent Gravier, Xavier Hoffer, and Jean-Philippe Ansermet

Institut de Physique des Nanostructures, Ecole Polytechnique Fédérale de Lausanne, CH-1015 Lausanne-EPFL, Switzerland

*present address: *Department of Materials Science and Engineering, Nagasaki University, Bunkyomachi 1-14, Nagasaki 852-8521, Japan*

(e-mail: ohgai@net.nagasaki-u.ac.jp, Tel & Fax: +81-95-819-2638)

Keywords: nanowire, electrodeposition, semiconductor, magnetoresistance, CdTe, NiFe

Abstract

Cylindrical nano-pores of an anodized aluminum oxide layer on the surface of bulk aluminum were used as templates for the electrochemical growth of semiconductor and magnetic nanowires. Electrodeposition process of CdTe and NiFe were investigated to determine the optimum conditions for each nanowire growth at the wide range of cathode potential. The desired composition of $Cd_{50}Te_{50}$ and $Ni_{80}Fe_{20}$ was achieved by controlling the cathode potential during the electrodeposition of nanowires. Temperature dependences of resistance for CdTe nanowires confirmed the semiconductor character with amorphous behavior at low temperature, while those of NiFe nanowires showed metallic character. Anisotropic magnetoresistance (AMR) of NiFe nanowires reached to 1.9% at 300K.

INTRODUCTION

Electron transport properties of nanowires have been received much attention due to the novel physical phenomenon and application to the new electronics materials. Recently, several research works have been reported on "magnetic or semiconductor nanowires" electrodeposited into nanoporous templates [1-6] for the purpose of application to the magnetic sensor, memory cell, photovoltaic, light emission diode (LED), etc. Using commercially available ion-track etched polycarbonate membrane filters or anodized aluminum oxide membrane filters, Bi_2Te_3 [4], CdTe [5] and PbSe [6] semiconductor nanowires or Co/Cu [7-9], NiFe/Cu [10] and CoNiCu/Cu [11] multilayered magnetic nanowires have been synthesized and characterized. Recently, M. Zenger *et al.* reported on the electrodeposition of NiFe and Fe nanopillars using PMMA template synthesis technique [12]. In this report, the single domain character of NiFe nanopillar has been demonstrated. The electrochemical growth of these nanowires started from a conductive metallic layer such as Au or Cu sputtered on one side of these membrane filters form.

Using anodized aluminum oxide pores on the surface of bulk aluminum, CdS semiconductor nanowires [13] or Ni, Co and Fe magnetic nanowires [14-18] have been also synthesized and characterized so far. Electrodeposition of nanowires into the anodized aluminum oxide pores can be carried out if an alternating current is applied to reduce the charging up effect of the barrier layer at the pore bottom. For the investigation of electron transport properties of nanowires, this resistive barrier layer should be removed to achieve good electric contacts at the pore bottom. It is well known that the barrier layer can be removed from the substrate side direction by dissolving the massive metallic aluminum backing [19-21]. However, since the thickness of barrier layer is assumed to be around several tens of

nm, this layer can be removed or thinned using a chemical etching technique from the pore side direction without dissolving the aluminum substrate [22-24].

Aluminum has been conventionally used in the field of civil architecture as well as microelectronics. As construction and building materials, aluminum shows excellent physical and chemical properties such as lightweight, mechanical strength and corrosion resistance. While, as an interconnect metal and wiring material, aluminum is applied in an ultra large scale integration (ULSI) processing. If anodization of aluminum and electrodeposition of semiconductor (SEMI) or magnetic (MAG) nanowires can be directly applied to the pores of aluminum surface, the template synthesis technique will be most promising candidate not only in the mass-production of solar cell panels, LED display, hybrid ULSI, etc., but also in the fundamental study of magnetic semiconductor such as MAG/SEMI multilayered or MAG-SEMI alloy type (NiFeCdTe, CoCdTe, etc.) novel nanowires.

In this study, we report on the fabrication of templates with cylindrical nano-pores using anodized aluminum oxide layer at the surface of bulk aluminum. CdTe semiconductor nanowires and NiFe ferromagnetic nanowires were electrodeposited into the nano-porous templates and the temperature dependence of resistance was examined to investigate the electron transport properties of the nanowires. Mott-Davis plots on CdTe nanowires and anisotropic magnetoresistance (AMR) on NiFe nanowires were also investigated.

EXPERIMENTAL PROCEDURE

Template Synthesis

Figure 1 (left-side) shows the schematic images on fabrication process of anodized aluminum templates. As shown in this figure, commercially available aluminum sheets

(thickness: 0.5mm) were used as a starting material to prepare anodized aluminum templates. First, the aluminum sheets were electrochemically polished in a solution of ethanol and perchloric acid (75 vol.% of ethanol, 25 vol.% of perchloric acid) to achieve a mirror-like surface. During the electrochemical polishing, the cell voltage was kept at 8V for 10 minutes. Then, the polished aluminum sheets were anodized in an aqueous solution containing 0.3 mol/L oxalic acid to obtain a nano-porous aluminum oxide layer on the surface. The cell voltage was kept at 50V for 10 minutes during anodization.

Figure 1 (right-side) shows the SEM images of a pore top planar view (Fig.1-(a)), a cross-sectional view (Fig.1-(b)) and a pore bottom back side view (Fig.1-(c)) of an anodized aluminum template. For the observation of pore bottom back side (*barrier layer*), the massive metallic aluminum substrate was dissolved in hydrochloric acid containing small amount of cupric ions (1.6 g/L $CuSO_4 \bullet 5H_2O$). The pore diameter is approximately 60nm and the pore density is of the order of 10^{10} pores/cm^2 as shown in Fig.1-(a), while the oxide layer had a typical porous columnar structure (Fig.1-(b)) and the pore length was approximately 2000nm. The existence of a barrier layer is made obvious by looking at the pore bottom of anodized aluminum oxide layer (Fig.1-(c)). To remove or thin this barrier layer without dissolving the metallic aluminum backing, the anodized aluminum templates were subsequently immersed in an aqueous solution containing 5 vol.% of phosphoric acid for 50 minutes prior to the electrodeposition process. For the electrodeposition of CdTe into the anodized aluminum templates, small amount of Cu (around 10nm thickness) was electrodeposited at the pore bottom to assist the electric contact of CdTe with aluminum substrate. A thin gold layer (thickness: 50nm), which serves as an *in-situ* electrical contact for the one of grown NiFe nanowires, was sputtered on the surface of the templates. This layer was thin enough to leave

the pores open. For the electrical contact of CdTe nanowires, the thin gold contact layer was sputtered after the electrodeposition of CdTe to make parallel contacts with multiple nanowires.

Nanowire Growth and Resistance Measurement

For the electrodeposition of CdTe and NiFe nanowires into the anodized aluminum templates, electrolytic solutions were prepared with ion-exchanged water containing following chemicals. *CdTe Bath*: $3CdSO_4 \bullet 8H_2O$ 25.6 g/L (Cd^{2+}: 0.1 mol/L), TeO_2 1.6 g/L (0.01 mol/L), and H_2SO_4 98 g/L (1.0 mol/L). *NiFe Bath*: $NiSO_4 \bullet 6H_2O$ 120 g/L (0.457 mol/L), $FeSO_4 \bullet 7H_2O$ 6.0 g/L (0.0215 mol/L), and H_3BO_3 45 g/L (0.728 mol/L). Cathodic polarization curves were measured at a wide potential range to determine the optimum conditions for CdTe and NiFe deposition. The nanowires were electrodeposited potentio-statically at the optimized potentials using a PC-controlled potentiostat and the composition of each deposit was determined using EDX analyzer.

Temperature dependence of the resistance on each nanowire was measured at the range from 10K to 300K using a cold-finger cryostat system. Magnetoresistance of NiFe nanowires was measured at 300K using a lock-in amplifier detection system, applying a 1μA current and sweeping the applied magnetic field slowly up to 10 kOe.

RESULTS AND DISCUSSION

Electrodeposition of Nanowires into Nano-porous Templates

Figure 2-(a) shows a cathodic polarization curve of an anodized aluminum template in the solution containing Cd^{2+} and $HTeO_2^+$ ions (*CdTe Bath*). The equilibrium potentials of Te

(E^{eq}_{Te}), CdTe (E^{eq}_{CdTe}) and Cd (E^{eq}_{Cd}) are estimated to be around +0.32V, –0.12V and -0.63V (vs.Ag/AgCl) based on the following electrochemical reactions.

$$HTeO_2^+ + 3H^+ + 4e^- = Te + 2H_2O \text{ - - - - - (1)}$$

$$Cd^{2+} + Te + 2e^- = CdTe \text{ - - - - - - - - - - - - (2)}$$

$$Cd^{2+} + 2e^- = Cd \text{ - - - - - - - - - - - - - - - - - (3)}$$

As shown in this figure, the cathodic current occurs and increases at around 0~0.1V and this current seems to correspond to the electrodeposition of Te (equation (1)) and CdTe (equation (2)). Recently, M. S. Martin-Gonzalez *et al.* reported on the electrodeposition process of Bi_2Te_3 [25]. Based on their cyclic voltammogramic study, the deposition potentials of Te and Bi_2Te_3 were determined to be less-noble than 0.19V and 0.05V. Also, M. Takahashi *et al.* reported on the electrodeposition process of CdTe with Cu-doping [26]. According to their cathodic voltammogramic study, the deposition potentials of Te and CdTe were determined to be less-noble than 0.07V and 0.20V. These reported results are in good agreement with those observed in this study. With increasing the cathodic current, at around 100A/m^2, the potential shifts to the less-noble direction. This phenomenon can be explained by the formation of resistive semiconductor phase (equation (2)) and the diffusion control of $HTeO_2^+$ ions. At the potential region close to E^{eq}_{Cd}, the cathodic current increases again at around –0.6V. It is well known that Cd^{2+} ions begin to electrodeposit without an accompanying overpotential from the aqua ions. In the sulfuric acid aqueous solution used in this study, Cd^{2+} ions exist as simple aqua ions. Therefore, this increase of cathodic current corresponds to the electrodeposition of Cd (equation (3)).

Figure 2-(b) shows Cd-content in the deposits obtained at various cathode potentials. The Cd-content increases with increasing cathode potential, and at the potential more noble than

–0.3V, Te-rich deposits are obtained, while Cd-rich deposits are obtained at the potential less noble than –0.5V. At the potential range of –0.3~-0.5V, stoichiometric composition (1:1) of CdTe deposits can be realized. It is well known that the co-deposition of Cd with Te proceeds based on the underpotential deposition of Cd and the results obtained in this study also could be explained due to the induced codeposition mechanism reported by Kröger [27].

Figure 3-(a) shows the polarization curves of mixed solution containing Ni^{2+} ions and Fe^{2+} ions (*NiFe Bath*; black line) and single solution containing 0.457mol/L of Ni^{2+} ions (gray line). The equilibrium potentials of Ni (E^{eq}_{Ni}) and Fe (E^{eq}_{Fe}) are estimated to be around -0.46V and –0.64V (vs.Ag/AgCl) based on the following electrochemical reactions.

$$Ni^{2+} + 2e^- = Ni \text{ - - - - - - - - - - (4)}$$

$$Fe^{2+} + 2e^- = Fe \text{ - - - - - - - - - - (5)}$$

In the Ni single solution, cathodic current occurs at around –0.1V, which is more noble than E^{eq}_{Ni}. This current is considered to be hydrogen evolution reaction at the cathode. With increasing the cathodic current, the cathode potential shifts to the less noble direction due to the diffusion control of hydrogen ions. At the potential region less noble than E^{eq}_{Ni}, the cathodic current increases again at around –0.6V. Iron-group metals such as Ni, Co and Fe electrodeposit accompanying with a significant overpotential caused by the rate determining of multi-step reduction even from the aqua ions. Therefore, this increase of cathodic current is considered as the deposition current of Ni. On the other hand, in Ni and Fe mixed solution (*NiFe Bath*), the deposition current of Ni occurs at around –0.8V, which is quite less noble than that of Ni single solution. It is well known that Ni deposition is suppressed by the existence of Fe^{2+} ions and less noble Fe preferentially deposits rather than Ni [28]. Therefore, the polarization of Ni deposition due to Fe^{2+} ions, which is observed in this study, can be

explained by the anomalous codeposition mechnism reported by Dahms, *et al* [28].

Figure 3-(b) shows Fe-content in the deposits obtained at various cathode potentials. The Fe-content increases with increasing cathode potential up to –1.1~-1.2V, and at the potential region less noble than –1.2V, Fe-content decreases with increasing cathode potential. This decrease of Fe-content would be caused by the diffusion control of Fe^{2+} ions. At the potential range of –1.1~-1.2V, permalloy composition ($Ni_{80}Fe_{20}$) of NiFe deposits can be realized.

Based on the polarization curves and the composition analysis of nanowires obtained in this study, the optimum conditions for $Cd_{50}Te_{50}$ nanowire growth are determined to be around -0.3~-0.5V, that is, at the potentials more noble than E^{eq}_{Cd} to avoid the codeposition of metallic Cd with CdTe. The optimum condition for $Ni_{80}Fe_{20}$ nanowire growth is determined to be around –1.1~1.2V, that is, at the potentials more noble than the diffusion control region of Ni^{2+} and Fe^{2+} ions.

Figure 4 shows SEM images of CdTe nanowire (a), (b) and NiFe nanowire (c) separated from nano-porous anodized aluminum oxide layer. The nano-porous template was dissolved in 5N-NaOH solution to observe CdTe and NiFe nanowires. As shown in these images, the nanowires have cylindrical shape with a large aspect ratio, and the sizes of diameter and length are corresponds well to those of the nano-porous template.

Electron Transport Properties of CdTe and NiFe nanowires

Figure 5-(a) shows the temperature dependence of resistance on CdTe nanowires electrodeposited at –0.5V. As shown in this figure, the resistance of CdTe nanowires presents an exponential increase with decreasing temperature, indicating their semiconductor character. When the nanowires were electrodeposited at less noble potential than –0.5V, for example at -

0.6V and -0.7V, the increase of resistance at low temperature region was not so remarkable as those obtained at –0.5V, due to the excess of co-deposited metallic Cd. The activation energy E_a was determined, using the usual relation for the conductivity σ in semiconductors:

$$\sigma = \sigma_0 \exp(-E_a/kT) \text{ - - - - - - - - - - (6)}$$

E_a is not constant over the temperature range. The maximum value found at room temperature is 19 meV for an electrodeposition potential of –0.5V. This value is far from the bandgap energy (E_g^{CdTe}=1.44eV), but typical localised states in the bandgap due to impurities and defects. Compared to tabulated values, it is in-between values of CdTe (some tens of meV) [29] and Te (a few meV) [30].

The temperature dependence of the resistance at low temperature (14K~120K) is analysed in regards with the Mott-Davis model [31] (Fig.5-(b)).

$$\sigma = \sigma_0 T^{-1/2} \exp(-BT^{-1/4}) \text{ - - - - - - - - - - (7)}$$

As shown in this figure, the experimental data is well fitted by the Mott-Davis plot at low temperature. This result suggests that the electrodeposited CdTe nanowires are composed from amorphous phase and the electron transport is based on *hopping conduction* mechanism [32, 33].

Figure 6-(a) shows the temperature dependence of resistance on NiFe nanowires electrodeposited at –1.2V. As shown in this figure, the resistance of NiFe nanowires decreases linearly with decreasing temperature and this temperature dependence confirms that the sample has a typical metallic character. Fig. 6-(b) shows magnetoresistance curves of NiFe nanowires electrodeposited at –1.2V. Here, MR ratio was defined as the following.

$$\text{MR ratio} = 100 (R_{max} - R_{min}) R_{min}^{-1} \text{ - - - - - (8)}$$

The resistance of NiFe nanowires strongly depends on the magnetic field direction and the

AMR reaches up to 1.9% at 90 degree (perpendicular magnetic field against to the wire axis). The saturating field is estimated to be around 5kOe, which is smaller than that of typical Ni nanowires. The inset-figure shows the close-up data of AMR hysteresis curve of NiFe nanowire measured at 60 degree. In this figure, a resistance jump was observed at 1.25 kOe with increasing magnetic field. This phenomenon confirms that a single nanowire is electrically contacted in the anodized aluminum template. According to the experimental results obtained in this study, it is confirmed that the pore bottom treatment technique using phosphoric acid is quite effective to remove most or all of the barrier layer and to make a good metallic electrical contact between aluminum substrate and electrodeposited nanowires.

CONCLUSION

CdTe and NiFe nanowires were fabricated on the surface of bulk aluminum using anodization and electrodeposition techniques. According to the temperature dependence of the resistance, CdTe nanowires obviously showed semiconductor characteristics. Mott-Davis plots at low temperature suggested that the electrodeposited CdTe nanowires are composed from amorphous phase and the electron transport is based on *hopping conduction* mechanism. NiFe nanowires showed clear metallic characteristics on the temperature dependence of the resistance. 1.9% of AMR response for NiFe single nanowire was successfully observed in anodized aluminum templates.

ACKNOWLEDGEMENTS

This work was supported in part by the Swiss Commission for Technology and Innovation (CTI) through the Technology Oriented Program - Nanometer in the 21st Century,

TOP-NANO21 (contract CTI no. 5812.1 TNS) and the European Commission (EC) through the Human Potential Program - Research Training Network (HPRN), European Network on Ion Track Technology, EuNITT (contract no. HPRN-CT-2000-00047).

REFERENCES

1. C. R. Martin, *Adv. Mater.* **3**, 457 (1991).
2. D. Aimawlawi, N. Coombs, and M. Moskovits, *J. Appl. Phys*. **70**, 4421 (1991).
3. T. M. Whitney, J. S. Jiang, P. C. Searson, and C. L. Chien, *Science* **261**, 1316 (1993).
4. A. L. Prieto, M. S. Sander, M. S. Martin-Gonzalez, R. Gronsky, T. Sands, and A. M. Stacy, *J. Am. Chem.Soc. Mater.* **123**, 7160 (2001).
5. D. Xu, Y. Guo, D. Yu, G. Guo, Y. Tang, and D. P. Yu, *J. Mater. Res*. **17**, 1711 (2002).
6. X. S. Peng, G. W. Meng, J. Zhang, X. F. Wang, C. Z. Wang, X. Liu, and L. D. Zhang, *J. Mater. Res*. **17**, 1283 (2002).
7. L. Piraux, J. M. George, J. F. Despres, C. Leroy, E. Ferain, R. Legras, K. Ounadjela, and A. Fert, *Appl. Phys. Lett*. **65**, 2484 (1994).
8. A. Blondel, J. P. Meier, B. Doudin, and J.-Ph. Ansermet, *Appl. Phys. Lett*. **65**, 3019 (1994).
9. K. Liu, K. Nagodawithana, P. C. Searson, and C. L. Chien, *Phys. Rev. B* **51**, 7381 (1995).
10. S. Dubois, C. Marchal, J. M. Beuken, L. Piraux, J. L. Duvail, A. Fert, J. M. George, and J. L. Maurice, *Appl. Phys. Lett*. **70**, 396 (1997).
11. G. P. Heydon, S. R. Hoon, A. N. Farley, S. L. Tomlinson, M. S. Valera, K. Attenborough, and W. Schwarzacher, *J. Phys. D: Appl. Phys*. **30**, 1083 (1997).
12. M. Zenger, W. Breuer, M. Zölfl, R. Pulwey, J. Raabe, and D. Weiss, *IEEE Trans. Magn*. **37**, 2094 (2001).

13. D. Routkevitch, T. Bigioni, M. Moskovits, and J. M. Xu, *J. Phys. Chem*. **100**, 14037 (1996).

14. F. Li and R. M. Metzger, *J. Appl. Phys*. **81**, 3806 (1997).

15. H. Zeng, M. Zheng, R. Skomski, D. J. Sellmyer, Y. Liu, L. Menon, and S. Bandyopadhyay, *J. Appl. Phys*. **87**, 4718 (2000).

16. Y. Peng, H. L. Zhang, S. L. Pan, and H. L. Li, *J. Appl. Phys*. **87**, 7405 (2000).

17. P. Forrer, F. Schlottig, H. Siegenthaler, and M. Textor, *J. Appl. Electrochem*. **30**, 533 (2000).

18. A. J. Yin, J. Li, W. Jian, A. J. Bennett, and J. M. Xu, *Appl. Phys. Lett*. **79**, 1039 (2001).

19. H. Masuda and K. Fukuda, *Science* **268**, 1466 (1995).

20. H. Masuda, H. Yamada, M. Satoh, H. Asoh, M. Nakao, and T. Tamamura, *Appl. Phys. Lett*. **71**, 2770 (1997).

21. O. Jessensky, F. Müller, and U. Gösele, *Appl. Phys. Lett*. **72**, 1173 (1998).

22. A. Tayaoka, E. Tayaoka, and J. Yamasaki, *J. Appl. Phys*. **79**, 6016 (1996).

23. K. Nielsch, F. Müller, A. P. Li, and U. Gösele, *Adv. Mater*. **12**, 582 (2000).

24. T. Ohgai, X. Hoffer, L. Gravier, J.-E. Wegrowe, and J.-Ph. Ansermet, *Nanotechnology*, **14,** 978 (2003).

25. M. S. Martin-Gonzalez, A. L. Prieto, R. Gronsky, T. Sands, and A. M. Stacy, *J. Electrochem. Soc*. **149**, C546 (2002).

26. M. Takahashi, Y. Muramatsu, M. Watanabe, K. Wakita, T. Miyuki, and S. Ikeda, *J. Electrochem. Soc*. **149**, C311 (2002).

27. F. A. Kröger, *J. Electrochem. Soc*. **125**, 2028 (1978).

28. H. Dahms and I. M. Croll, *J. Electrochem. Soc*. **112**, 771 (1965).

29. G. Nimtz, in *Physics of II-VI and I-VII Compounds, Semimagnetic Semiconductors*, Landolt-Börnstein, New Series, Group 3, Vol.17b, edited by O. Madelung (Springer-Verlag, Berlin 1982) p.225.

30. P. Gross and W. Richter, in *Physics on Non-Tetrahedrally Bonded Elements and Binary Compounds*, Landolt-Börnstein, New Series, Group 3, Vol.17e, edited by O. Madelung (Springer-Verlag, Berlin 1983) p.106.

31. A. I. Kolyubakin, V. E. Antonov, O. I. Barkalov, A. F. Gurov, and A. I. Harkunov, *J. Non-Cryst. Solids* **289**, 30 (2001).

32. M. A. Majeed Khan, M. Zulfequar, and M. Husain, *J. Mater. Sci.* **38**, 549 (2003).

33. N. F. Mott, *Phil. Mag.* **22**, 7 (1970).

Figure Captions

Fig.1 Fabrication process of anodized aluminum template (left-side). SEM images of pore top plan view (a), cross sectional view (b) and pore bottom plan view (c) of anodized aluminum template. Anodized aluminum oxide layer has a typical porous columnar structure and the pore-length is approximately 2000 nm. The pore-diameter is approximately 60 nm.

Fig.2 Cathodic polarization curve of anodized aluminum templates in the solution containing $HTeO_2^+$ ions and Cd^{2+} ions (a). Cd-content in deposits obtained at various cathode potentials (b).

Fig.3 Cathodic polarization curves of anodized aluminum templates in the solution containing Ni^{2+} ions and Fe^{2+} ions (a). Fe-content in deposits obtained at various cathode potentials (b).

Fig.4 SEM images of CdTe nanowire (a), (b) and NiFe nanowire (c) separated from nano-porous anodized aluminum oxide layer.

Fig.5 Temperature dependence of resistance at 10K~300K (a) and the Mott-Davis plots at low temperature region of 14K~120K (b) on CdTe nanowires electrodeposited at –0.5V.

Fig.6 Temperature dependence of resistance (a) and magnetoresistive hysteresis (b) on NiFe nanowires electrodeposited at -1.2V. (Inset-figure shows the close-up data of AMR hysteresis measured at 60^o).

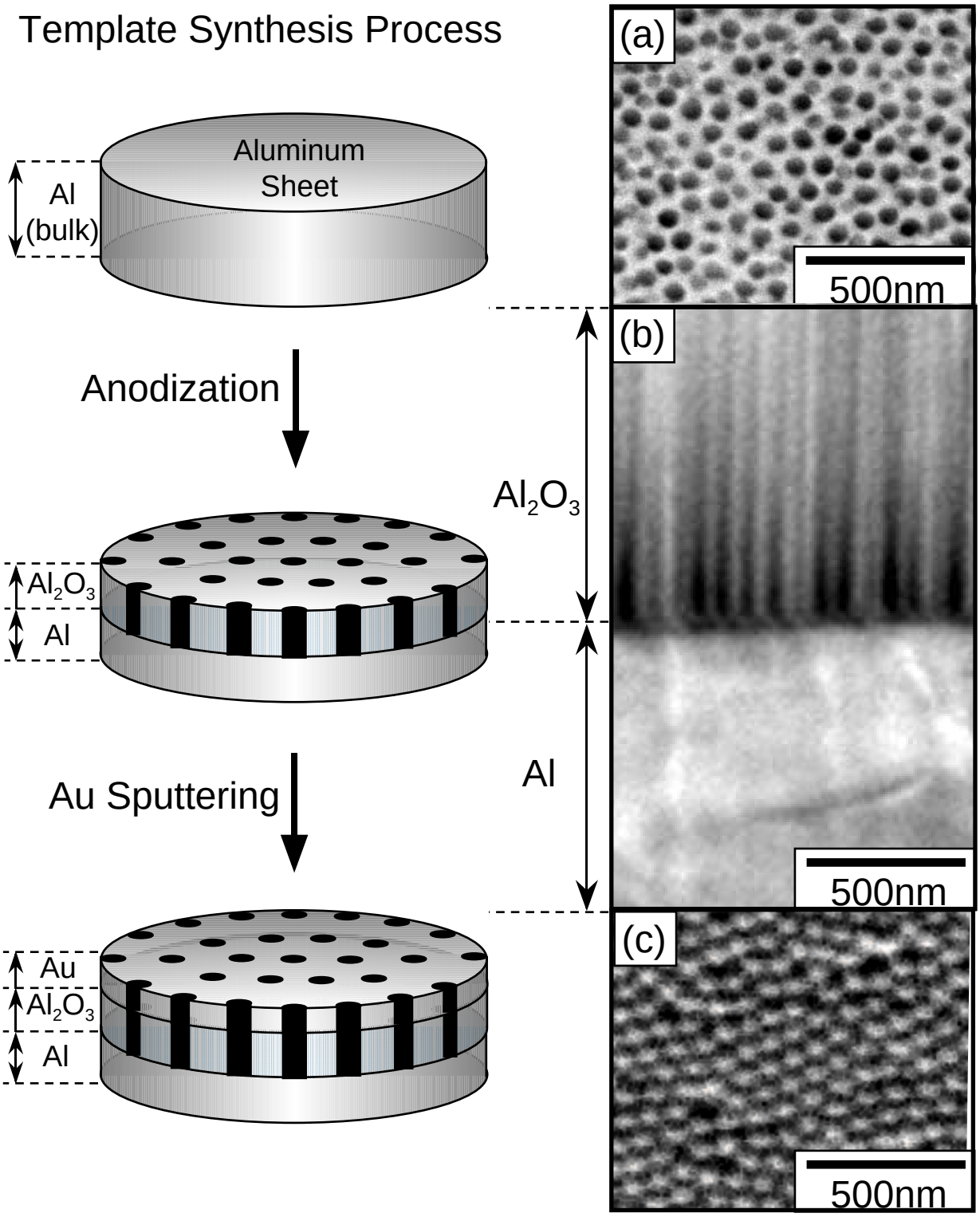

Fig.1 Fabrication process of anodized aluminum template (left-side). SEM images of pore top plan view (a), cross sectional view (b) and pore bottom plan view (c) of anodized aluminum template. Anodized aluminum oxide layer has a typical porous columnar structure and the pore-length is approximately 2000 nm. The pore-diameter is approximately 60 nm.

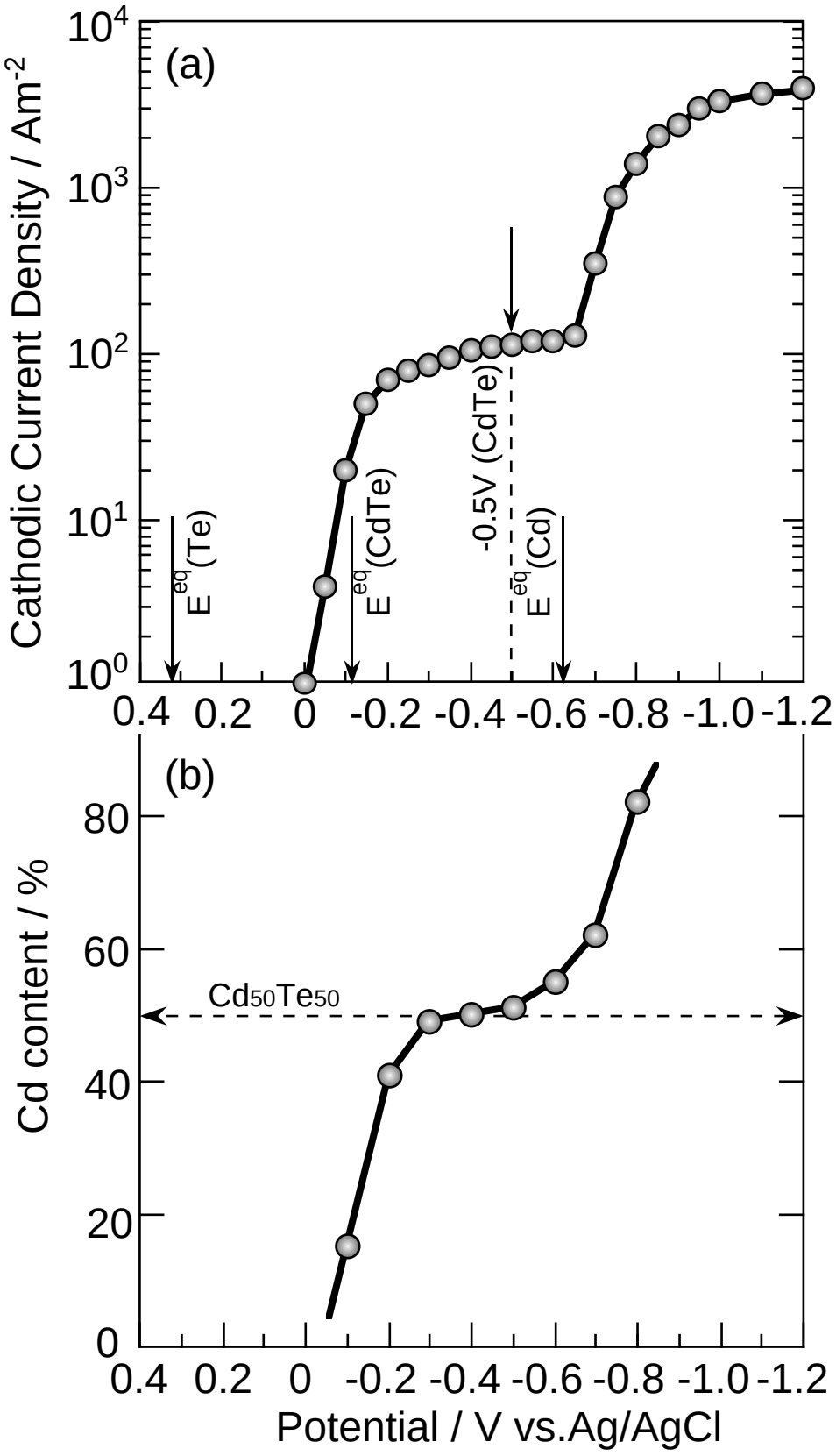

Fig.2 Cathodic polarization curve of anodized aluminum templates in the solution containing $HTeO_2^+$ ions and Cd^{2+} ions (a). Cd-content in deposits obtained at various cathode potentials (b).

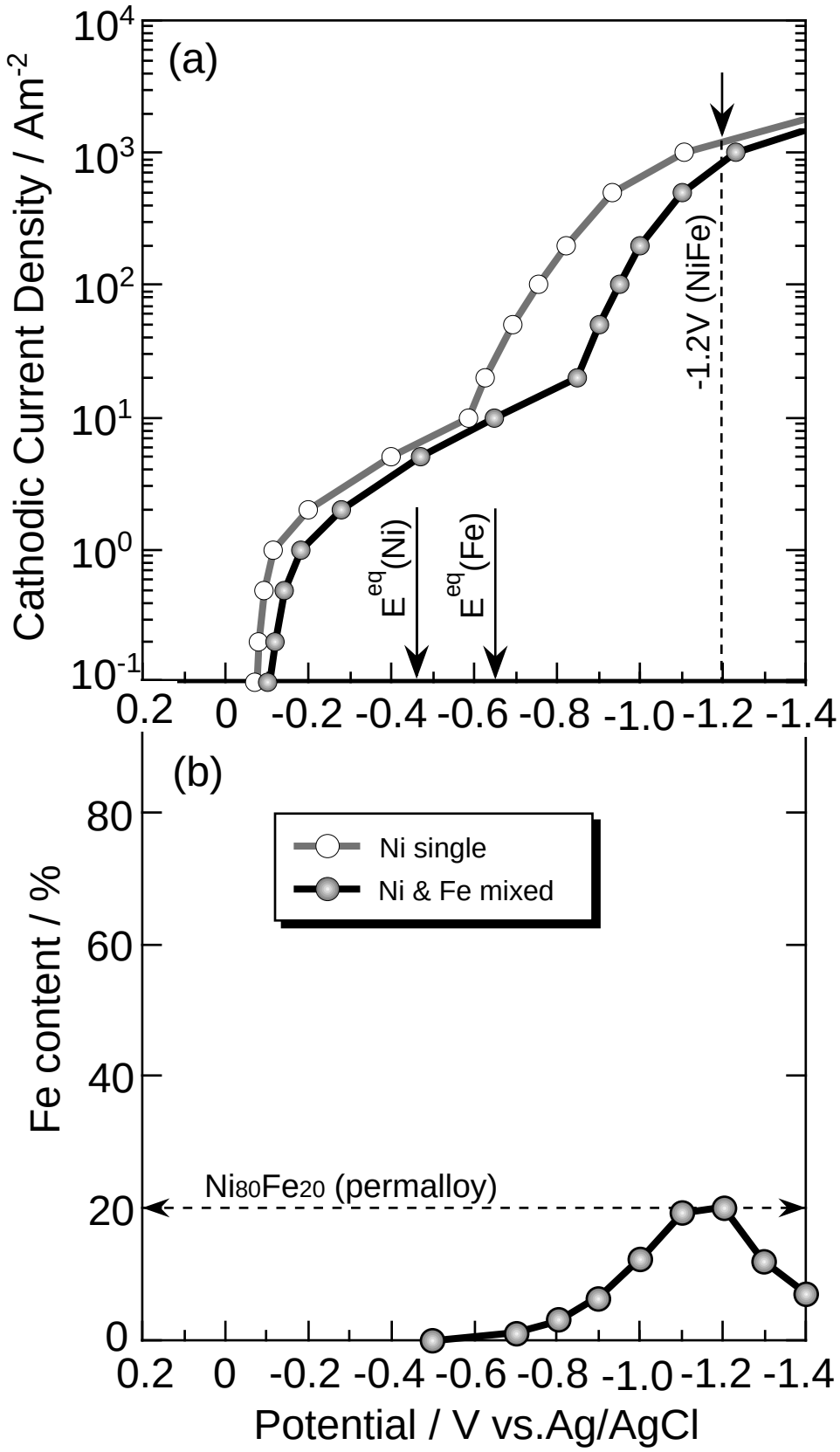

Fig.3 Cathodic polarization curves of anodized aluminum templates in the solution containing Ni^{2+} ions and Fe^{2+} ions (a). Fe-content in deposits obtained at various cathode potentials (b).

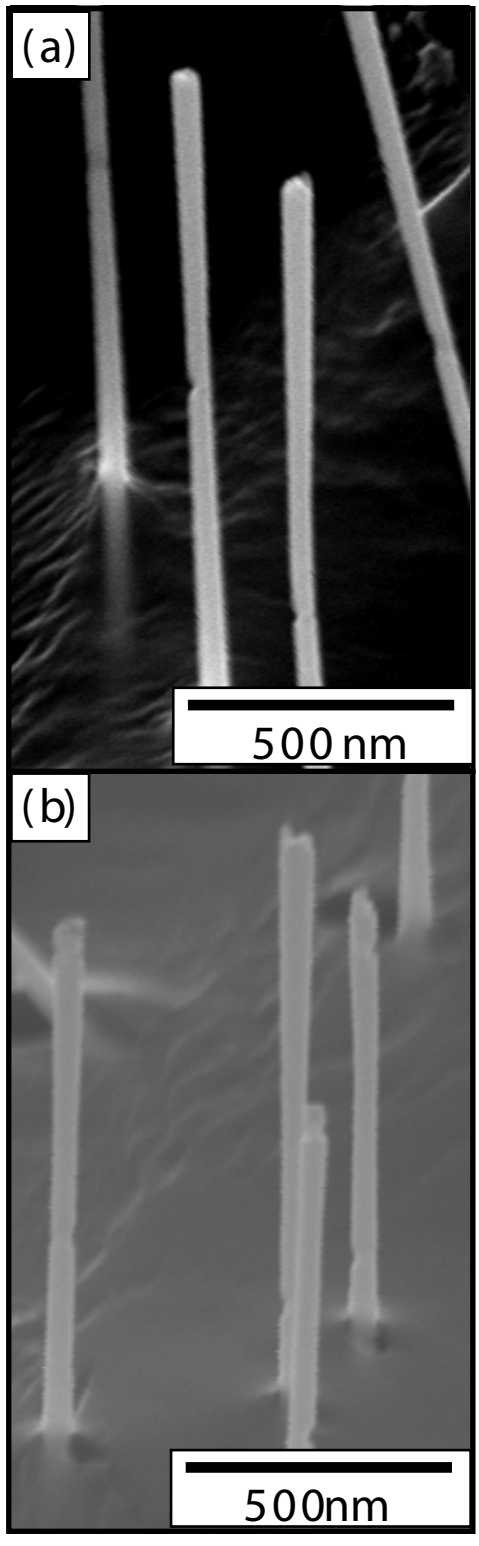

Fig.4 SEM images of CdTe nanowires (a) and NiFe nanowires (b) separated from nano-porous anodized aluminum oxide layer.

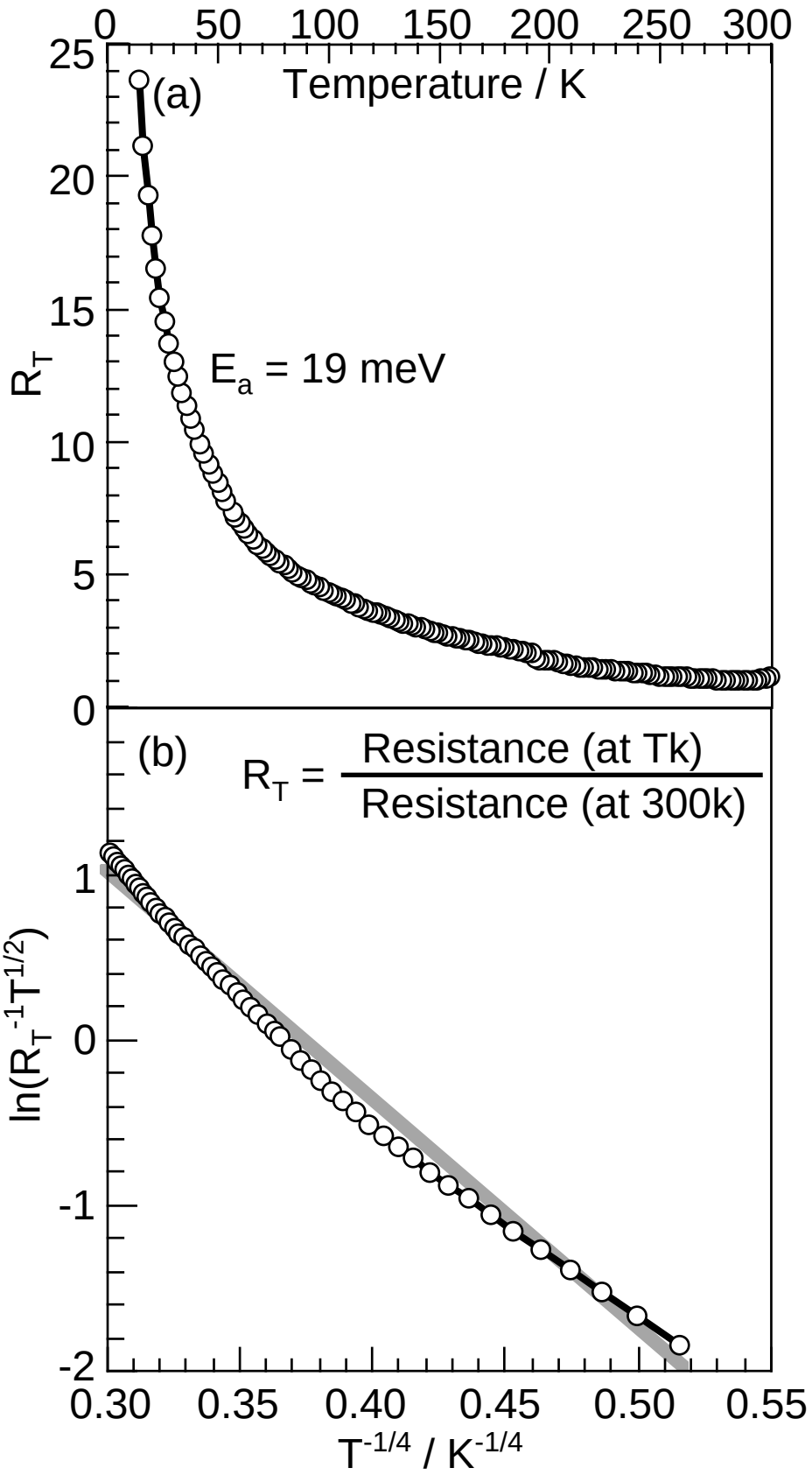

Fig.5 Temperature dependence of resistance at 10K~300K (a) and the Mott-Davis plots at low temperature region of 14K~120K (b) on CdTe nanowires electrodeposited at -0.5V.

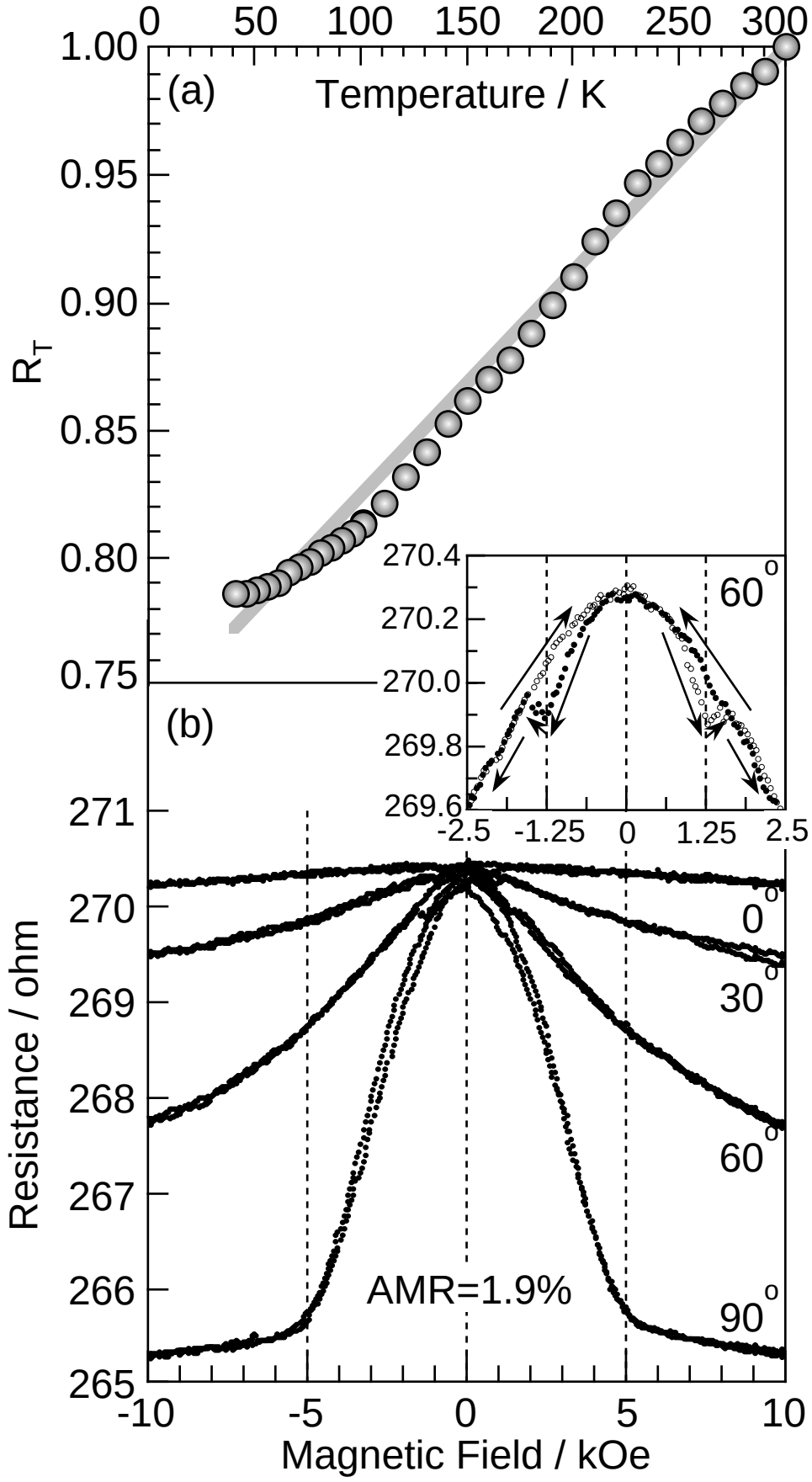

Fig.6 Temperature dependence of resistance (a) and magnetoresistive hysteresis (b) on NiFe nanowires electrodeposited at -1.2V. (Inset-figure shows the close-up data of AMR hysteresis measured at 60^o)